arXiv:1409.0432v1 [cond-mat.supr-con] 1 Sep 2014

Magnetic structure of the Eu^{2+} moments in superconducting $EuFe_2(As_{1-x}P_x)_2$ with $x = 0.19$

S. Nandi,[1,2,*] W. T. Jin,[1,2] Y. Xiao,[1] Y. Su,[2] S. Price,[1] W. Schmidt,[3] K. Schmalzl,[3] T. Chatterji,[4] H. S. Jeevan,[5,6] P. Gegenwart,[5,7] and Th. Brückel[1,2]

[1]*Jülich Centre for Neutron Science JCNS and Peter Grünberg Institut PGI, JARA-FIT, Forschungszentrum Jülich GmbH, D-52425 Jülich, Germany*
[2]*Jülich Centre for Neutron Science JCNS, Forschungszentrum Jülich GmbH, Outstation at MLZ, Lichtenbergstraße 1, D-85747 Garching, Germany*
[3]*Jülich Centre for Neutron Science, Forschungszentrum Jülich, Outstation at Institut Laue-Langevin, BP 156, 38042 Grenoble Cedex 9, France*
[4]*Institut Laue-Langevin, BP 156, 38042 Grenoble Cedex 9, France*
[5]*I. Physikalisches Institut, Georg-August-Universität Göttingen, D-37077 Göttingen, Germany*
[6]*Department of Physics, PESITM, Sagar Road, 577204 Shimoga, India*
[7]*Center for Electronic Correlations and Magnetism, Experimental Physics VI, Universität Augsburg, D-86135 Augsburg, Germany*

The magnetic structure of the Eu^{2+} moments in the superconducting $EuFe_2(As_{1-x}P_x)_2$ sample with $x = 0.19$ has been determined using neutron scattering. We conclude that the Eu^{2+} moments are aligned along the **c** direction below $T_C = 19.0(1)$ K with an ordered moment of $6.6(2)\,\mu_B$ in the superconducting state. An impurity phase similar to the underdoped phase exists within the bulk sample which orders antiferromagnetically below $T_N = 17.0(2)$ K. We found no indication of iron magnetic order, nor any incommensurate magnetic order of the Eu^{2+} moments in the sample.

PACS numbers: 74.70.Xa, 75.25.-j, 75.40.Cx

I. INTRODUCTION

In the last few years, there have been a flurry of research activity in the field of unconventional high-T_C superconductivity [1] due to the discovery of iron-based superconductors in 2008 [2]. Among various classes of Fe-based superconductors [2–7], the ternary "122" system, AFe_2As_2 (A = Ba, Ca, or Sr, etc) with T_C up to 38 K, [8–10], has been the most widely studied member of Fe-pnictide superconductors. $EuFe_2As_2$ is an interesting member of the "122" family since the A site is occupied by the Eu^{2+}, which is an S-state rare-earth ion possessing a $4f^7$ electronic configuration with the electron spin $S = 7/2$ [11]. $EuFe_2As_2$ exhibits a spin density wave (SDW) transition in the Fe sublattice concomitant with a structural phase transition at 190 K. In addition, Eu^{2+} moments order in an A-type antiferromagnetic (AFM) structure at 19 K (ferromagnetic layers ordered antiferromagnetically along the **c** direction) [12–14]. Superconductivity can be achieved in this system by substituting Eu with K or Na [9, 15], As with P [16], and upon application of external pressure [17–19]. Doping as well as external pressure lead to a decrease of both the structural and Fe magnetic phase transition temperatures and eventually superconductivity appears when both transitions are suppressed enough [9]. Upon P-doping, the ordering temperature of the Eu^{2+} moments initially decreases by a few Kelvin until the superconductivity appears and then increases up to 30 K as the doping is increased further [20].

The superconducting dome for the P-doped $EuFe_2As_2$ is quite narrow compared to the other Fe-based "122" pnictides [21]. It is generally accepted that the Eu^{2+} moments order antiferromagnetically before the superconducting dome and ferromagnetically after the superconductivity is suppressed [20]. However, the exact nature of the Eu^{2+} magnetic order within the superconducting dome remained controversial [22]. Most surprising is the coexistence of ferromagnetism and superconductivity as recently proposed by many groups for the P-doped $EuFe_2As_2$ samples [22–26]. In particular, Zapf *et al*. [22, 26] concluded based on macroscopic measurements that the Eu^{2+}moments in $EuFe_2(As_{1-x}P_x)_2$ order in a canted A-type antiferromagnetic structure with the spin component along the **c** direction being ferromagnetically aligned. Zapf *et al*. [22] also discovered that the A-type antiferromagnetic order of the Eu^{2+} moments below around 20 K undergoes a spin glass transition at lower temperatures where the in plane components of the magnetic moments are responsible for the glassy freezing.

For the superconducting $EuFe_2(As_{1-x}P_x)_2$ samples with $x = 0.15$, we have recently concluded that the Eu^{2+} moments are primarily aligned ferromagnetically along the **c** direction using x-ray resonant magnetic scattering [27]. However, due to the limited sensitivity of the x-ray scattering technique for the ferromagnetic structures, the moment size could not be determined from the previous studies. Neutron diffraction studies on a superconducting $Eu(Fe_{0.82}Co_{0.18})_2As_2$ single crystal revealed a long-range ferromagnetic order of the Eu^{2+} moments along the **c** direction [28]. Due to the strong neutron absorption of the natural Eu (~ 5800 barns at λ = 2.513 Å) together with the small sample mass (~ 10 mg) of the P-doped single crystals compared to the Co-doped $EuFe_2As_2$ (~100 mg), the magnetic structure determination in $EuFe_2(As_{1-x}P_x)_2$ via neutron diffraction is considerably more challenging. The only attempt was made on a powder sample of the non-superconducting end-member $EuFe_2P_2$ where it was concluded that the Eu^{2+} moments order ferromagnetically with a canting angle of 17° from the **c** axis [29]. Based on Mössbauer studies on superconducting poly-

crystalline samples, Nowik *et al.* [25] also concluded that the Eu^{2+} moments are aligned ferromagnetically along the **c** axis with a possible tilting angle of 20° from the **c** axis for $EuFe_2(As_{1-x}P_x)_2$ with $x \geq 0.2$. On the other hand, it was concluded for the Co-doped $EuFe_2As_2$ samples that the canting angle is nearly zero [28]. Therefore, it is very important to clarify the moment direction and the absolute value of the ordered moment using neutron diffraction for the P-doped $EuFe_2As_2$ single crystals with different doping levels. Here we report on the neutron scattering studies of the superconducting $EuFe_2(As_{1-x}P_x)_2$ single crystal with $x = 0.19$ to explore the details of the magnetic structure of the Eu^{2+} moments. Our neutron scattering experiments show that the Eu^{2+} moments order ferromagnetically along the **c** direction with an ordered moment of 6.6(2) μ_B. No magnetic order associated with Fe as well as no structural phase transition could be detected.

II. EXPERIMENTAL DETAILS

Single crystals of $EuFe_2(As_{1-x}P_x)_2$ with $x = 0.19$ were grown using FeAs flux [20]. For the scattering measurements, a 10 mg as-grown triangular shaped single crystal of approximate dimensions 2.9 mm×3.5 mm×3.8 mm and thickness of 0.3 mm was selected (see inset of Fig. 1) and it's phosphorous content was determined within 1% accuracy on four different spots by freshly cleaving the sample using EDX (Energy dispersive x-ray analysis). High-resolution elastic neutron scattering experiments were carried out on the cold-neutron triple-axis spectrometer IN12 at the high-flux reactor of the Institut Laue Langevin in Grenoble, France. Vertically focused Pyrolytic Graphite (PG) (0 0 2) monochromator and analyzer were used. In addition, monochromator was partially focused horizontally to optimize flux for the used collimators. To have a better q-space resolution, $60'$ collimators were used between the sample and the monochromator as well as between the sample and the analyzer. A velocity selector in the guide about 39 m upstream served as a second order filter and for background reduction. The measurements were carried out with fixed final wave vectors of k_f = 2.5 $Å^{-1}$ and 2.85 $Å^{-1}$, which corresponds to neutron wavelengths of 2.513 Å and 2.205 Å, respectively. Due to the geometrical limitation of the instrument, the shorter wavelength was employed only for the measurement of the (2 2 0) reflection. The larger wavelength was used for the rest of the measurements for improved flux. The single crystal was mounted on a Vanadium pin using very small amount of GE-Varnish and mounted inside an ILL orange type cryostat. Furthermore, the sample stick near the sample as well as the Vanadium pin was covered with a thick Cd foil for the reduction of background. Slits before and after the sample were used to further reduce the background. Initially measurements were performed in the $(1\ 1\ 0)_T$-$(0\ 0\ 1)_T$ scattering plane. Later, the sample was remounted in the $(1\ 0\ 0)_T$-$(0\ 0\ 1)_T$ scattering plane for measurements of more magnetic and nuclear reflections. Measurements at IN12 were performed at temperatures between 2 and 100 K. For convenience, we will use tetragonal (T) notation unless otherwise specified.

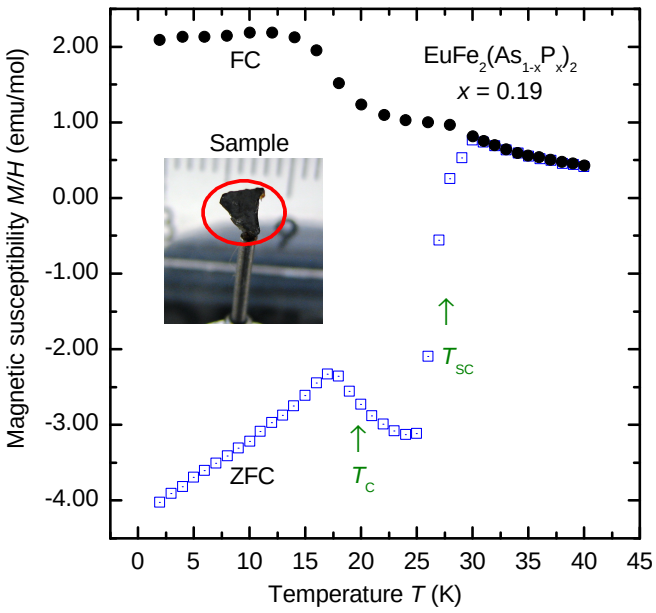

Figure 1: Temperature dependence of the magnetic susceptibility measured on heating of the zero-field cooled (ZFC) and field cooled (FC) sample along the a-b plane at an applied magnetic field of 25 Oe. T_{SC} and T_C denote superconducting and ferromagnetic transition temperatures, respectively. The transition temperatures were determined from the minima/maxima of the derivative curve of the ZFC data.

III. EXPERIMENTAL RESULTS

A. Macroscopic Characterizations

Figure 1 shows temperature dependence of the magnetic susceptibility M/H measured for magnetic field parallel to the a-b plane using a Quantum Design (SQUID) magnetometer. Zero field cooled magnetization becomes negative at T_{SC} = 27 K, signifying a superconducting transition at this temperature. At slightly lower temperature and at T_C = 19 K superconducting signal is weakened by the onset of the Eu^{2+} magnetic order and has been observed in heat-capacity measurements [20]. The transition at T_C is the ferromagnetic transition of Eu^{2+} moments as supported by the saturation of magnetization (FC susceptibility) as well as strong increase of the intensity for the nuclear reflections (see next section) below this temperature. Furthermore, it was found that the entropy release associated with this transition is close to the theoretical value of $R\ln(2S + 1)$ for the Eu^{2+} moments with spin S = 7/2 on similar chemical compositions [20, 27]. Superconductivity wins over the Eu^{2+} magnetism if temperature is lowered fur-

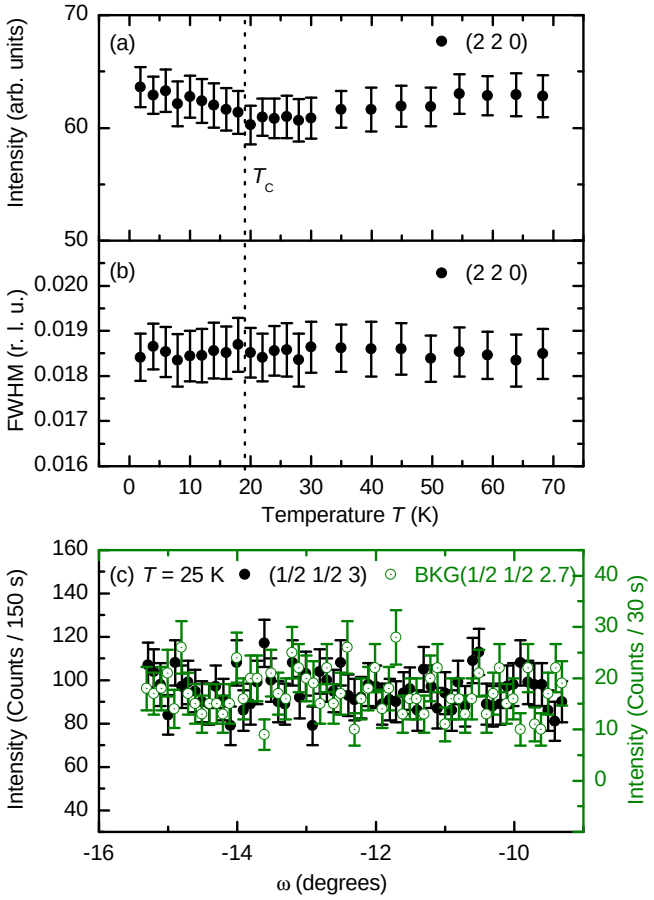

Figure 2: (a) Temperature dependence of the integrated intensity for the (2 2 0) reflection. (b) Temperature dependence of the Full-Width-Half-Maximum (FWHM) for the same reflection. (c) Rocking scans at the expected position of the Fe magnetic order at $(\frac{1}{2}\ \frac{1}{2}\ 3)$ at 25 K and at the background position of $(\frac{1}{2}\ \frac{1}{2}\ 2.7)$.

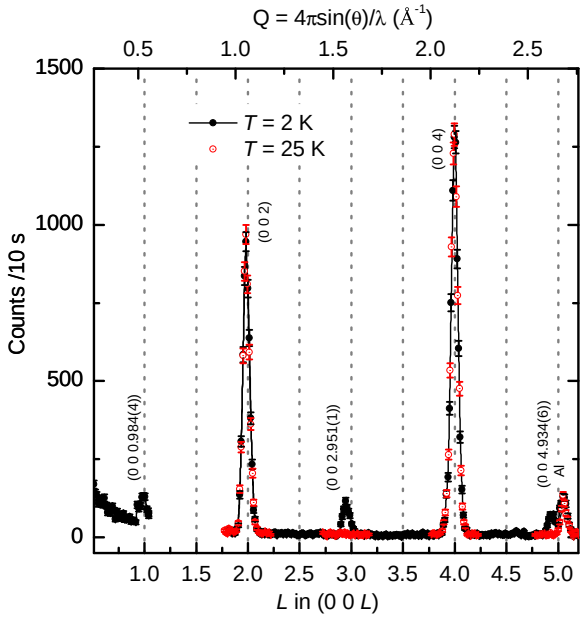

Figure 3: Scans along the [0 0 1] direction at T = 2 and 25 K, respectively. For the (0 0 1) reflection, measurement has been performed only at 2 K due to the technical difficulties. Break in measurement data between L = 1.1 and 1.75 is due to the same difficulties. The temperature independent peak near L = 5.04 is due to Aluminum (Al). The peak positions near the (0 0 L) with L = odd were determined after fitting the peaks using Gaussian profiles.

ther. The results of magnetic susceptibility are consistent with the published results of Jeevan *et al.* [20].

B. Neutron diffraction

It has been established for the parent compound as well as for the 15% P-doped samples that there is a structural phase transition from space group $I4/mmm$ to $Fmmm$, with a distortion along the [1 1 0] direction at 190 and 49 K, respectively [13, 27]. To determine whether there is a similar structural phase transition, (ξ ξ 0) scans were performed through the tetragonal (2 2 0) Bragg reflection as a function of temperature. Figure 2(a) shows temperature dependence of the integrated intensity for the (2 2 0) reflection as the sample was warmed up from 2 to 70 K. It can be seen that there is an increase of intensity below T_C = 19 K, coincident with the onset of the magnetic order of the Eu^{2+} moments. No change in intensity at higher temperatures associated with the extinction release [28] at the structural phase transition has been observed. Figure 2(b) shows temperature dependence of the Full-Width-Half-Maximum (FWHM) for the same reflection. However, the FWHM remains constant within the experimental error in the investigated temperature range and provides an upper limit of the structural distortion, $\delta = (a-b)/(a+b) \sim 2.5\times10^{-4}$. For comparison, we note that for the 15% doped sample a structural distortion of 5×10^{-4} was observed at T = 25 K [27].

For the undoped parent compound, the Fe moments order magnetically below 190 K with a propagation vector $\tau = (\frac{1}{2}\ \frac{1}{2}\ 1)$ [13]. Figure 2(c) shows ω scans (rocking curves) through the expected position of the strongest magnetic peak at $(\frac{1}{2}\ \frac{1}{2}\ 3)$ at 25 K and at the background position of $(\frac{1}{2}\ \frac{1}{2}\ 2.7)$. Similar scans were performed at 2 K and 40 K (not shown). However, we failed to observe any magnetic peak corresponding to the Fe magnetic order indicating the absence of the Fe magnetic order within our experimental accuracy.

For the parent compound, Eu^{2+} moments adopt an A-type antiferromagnetic structure characterized by the propagation vector $\boldsymbol{\tau} = (0\,0\,1)$. Figure 3 shows Q-scans along the [0 0 1] direction at T = 2 and 25 K, respectively. Very weak magnetic signals were observed at T = 2 K near (0 0 L) with L = odd compared to the allowed nuclear peaks at (0 0 L) with

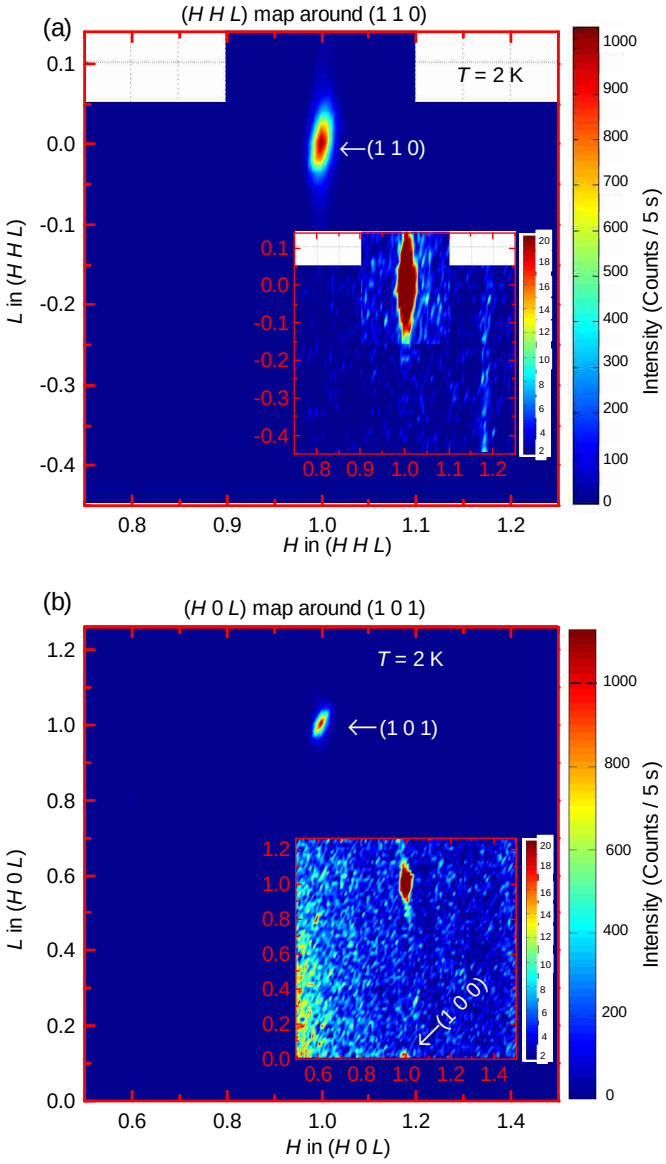
(a)
(H H L) map around (1 1 0)
T = 2 K
←(1 1 0)
L in (H H L)
H in (H H L)
Intensity (Counts / 5 s)
(b)
(H 0 L) map around (1 0 1)
T = 2 K
←(1 0 1)
←(1 0 0)
L in (H 0 L)
H in (H 0 L)
Intensity (Counts / 5 s)

Figure 4: (a) and (b) Two dimensional contour maps in the (*H H L*) and in the (*H* 0 *L*) planes at *T* = 2 K. Insets show both figures with different intensity scales to visualize weakest peaks, if any. No data were collected in the white rectangular region of Fig. (a). (1 1 0) and (1 0 1) are allowed nuclear peak positions. The weak peak at (1 0 0) indicates antiferromagnetic order of the Eu^{2+} moments with propagation vector τ = (0 0 1) associated with the minor phase.

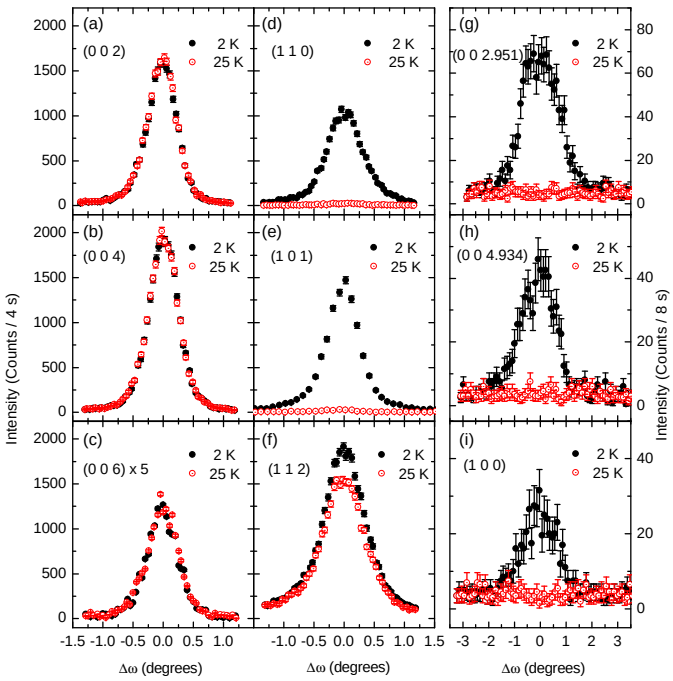
(a) (0 0 2) 2 K 25 K
(d) (1 1 0) 2 K 25 K
(g) (0 0 2.951) 2 K 25 K
(b) (0 0 4) 2 K 25 K
(e) (1 0 1) 2 K 25 K
(h) (0 0 4.934) 2 K 25 K
(c) (0 0 6) x 5 2 K 25 K
(f) (1 1 2) 2 K 25 K
(i) (1 0 0) 2 K 25 K
Intensity (Counts / 4 s)
Intensity (Counts / 8 s)
Δω (degrees)
Δω (degrees)
Δω (degrees)

Figure 5: Rocking scans for the (a-c) (0 0 2), (0 0 4) and (0 0 6) reflections, (d-f) (1 1 0), (1 0 1) and (1 1 2) reflections, and (g-i) (0 0 2.95), (0 0 4.95) and (1 0 0) reflections at 2 and 25 K, respectively. Note the intensity scales for the (0 0 *L*) reflections with *L* = odd and *L* = even.

L = even. One expects comparable intensities for the (0 0 2) nuclear peak and the (0 0 3) magnetic peak for the fully ordered moment of Eu^{2+} as observed for the parent compound [13]. The magnetic peaks are broader in *q*-space compared to the allowed nuclear peaks and appear at positions incommensurate with the nuclear peaks. However, this does not ensure that the magnetic structure is incommensurate with the lattice since the twin satellite peaks are absent. The observation of magnetic peaks at slightly lower *L* values (with *L* odd) might be due to the existence of a minor phase with *c* lattice parameter larger than the main phase. The shift of the peak positions of the (0 0 *L*) peaks with *L* = odd from the nearest integer values increases progressively with increasing *L* values. This is expected for a minor phase with a larger *c* lattice parameter. Based on the positions of the three magnetic peaks a modified *c* lattice parameter, *c*' = (1.016 ± 0.003) *c*, can be determined where *c* corresponds to the lattice parameter of the main phase. It is known that the decrease in *c* lattice parameter is more pronounced compared to the *a*/*b* lattice parameters as a result of chemical pressure by P-doping [20]. Hence, the peaks near (0 0 *L*) with *L* = odd might be associated with a minor phase similar to the undoped or underdoped phases. Here we note that we did not observe (0 0 2-2Δ) and (0 0 4-4Δ) peaks which is expected for the minor phase (Δ = 0.016). This might be due to the weakness of the signal from the minor phase (volume fraction only 1.5%, see next section) together with the close proximity of the lattice parameters with the main phase

Maps in the (*H H L*) and (*H* 0 *L*) planes were performed at *T* = 2 K to search for additional magnetic peaks. Figures 4(a) shows a two dimensional contour map around the very weak nuclear peak (1 1 0). Only the main nuclear peak was observed, however, with intensity comparable to the strongest nuclear peaks. Similar contour map around another weak nuclear peak (1 0 1) in the (*H* 0 *L*) plane was performed and

is shown in Fig. 4 (b). In addition to the nuclear peak at (1 0 1), a very weak magnetic peak was found at (1 0 0) characterized by the propagation vector $\boldsymbol{\tau}$ = (0 0 1) as observed before. Very strong intensity at the weakest nuclear peaks and the absence of incommensurate peaks indicate that the magnetic unit cell might be the same as the chemical unit cell with magnetic propagation vector $\boldsymbol{\tau}$ = (0 0 0). Therefore, rocking scans for several representative nuclear peaks at T = 2 and 25 K were performed to verify if there is any magnetic contribution superimposed on the nuclear peaks. These scans are shown in Figure 5 (a-f). It is clear from the ω scans of the (0 0 L) reflections with L = even in Figs. 5 (a-c) that they have identical intensities at 2 and 25 K, indicating the absence of magnetic signal at these positions. However, the weakest nuclear peaks, (1 1 0) and (1 0 1), in Figs. 5 (d-e) show very strong magnetic signals as the intensity of these reflections almost vanishes at 25 K. For the strong nuclear peak (1 1 2), magnetic signal can be observed on top of the nuclear signal as shown in Figs. 5 (f). The absence of magnetic intensity for the (0 0 L) reflections with L even as well as strong intensity at the (1 1 0) position indicates that the moments are primarily along the **c** direction. Figs. 5 (g-i) show ω scans of the magnetic peaks associated with the minor phase. The FWHM of the ω scans for the minor phase (~ 1.5°) are much larger than the main phase (~ 0.5°) indicating weak magnetic correlations or incoherently grown minor phase.

Figure 6(a) shows temperature dependencies of the integrated intensities for the (1 1 0) and (1 0 1) reflections. No hysteresis was observed between the heating and cooling cycles indicating second order nature of the phase transition. The integrated intensity ($I \sim m^2$, where m is the sublattice magnetization) can be fitted with a power law of the form $I \sim (1 - \frac{T}{T_C})^{2\beta}$ to obtain transition temperature of the Eu^{2+} magnetic order T_C = 19.0(1)K and an exponent $\beta = 0.36(4)$. Since the (1 0 1) reflection is sensitive to both in and out of plane magnetic components, the identical nature of the temperature dependencies for both reflections indicates that the spin canting out of plane, if any, remains constant over the whole temperature range. Figure 6 (b) shows temperature dependencies of the (0 0 2.95) and (1 0 0) magnetic reflections corresponding to the antiferromagnetic ordering of the Eu^{2+} moments associated with the minor phase. Using the same power law fitting to the integrated intensity, antiferromagnetic ordering temperature, T_N = 17.0(2), and $\beta = 0.27(3)$ could be obtained. The exponent for the main phase is close to that (0.36) (Ref. 30) of the three-dimensional 3D classical Heisenberg model, typical for rare-earth elements in intermetallic compounds [31, 32]. Surprisingly, the minor phase order magnetically at a slightly lower temperature than the major phase, further hinting towards two independent magnetic phases. A decrease in ordering temperature as has been observed for the underdoped region of the phase diagram might indicate that the minor phase is located in the underdoped region in the phase diagram [20, 22]. At low temperatures, the intensities of the reflections from the major and minor phases were fitted using FULLPROF [33] after necessary absorption correction using DATAP [34]. For the major phase, a ferromagnetic structure of the Eu^{2+} moments along the c direction was assumed (as concluded in the next section). The intensities of the minor phase (a total of eight magnetic reflections) were fitted with an A-type antiferromagnetic structure of the Eu^{2+} moments [13] with the moment size same as that of the major phase. Comparing the scale factors for the major phase and minor phase, we estimate the volume fraction of the minor phase to be (1.5 ± 0.4) % .

C. Magnetic structure of the Eu^{2+} moments

We now turn to the determination of the magnetic moment configuration for the Eu^{2+} moments in the major phase. Here we note that only ferromagnetic structures with magnetic moments along the three crystallographic directions **a**, **b**, **c** are allowed by symmetry. No antiferromagnetic structure with $\boldsymbol{\tau}$ = (0 0 0) is possible in this case for symmetry reasons. Since for magnetic neutron scattering, the scattered intensity is sensitive to the component of the magnetic moment perpendicular to **Q**, absence of magnetic intensity for the nuclear (0 0 L) reflections (see Figs. 5 (a-c)) indicates that the moments are primarily along the **c** direction. However, to put an upper limit on the canting angle as well as to determine the moment size, a magnetic structure refinement is needed. Conventional magnetic structure refinement using integrated intensity is difficult in this case because, (a) the number of measured reflections is limited due to the use of thermal neutrons in a triple axis spectrometer and, (b) the errors associated with the resolution effects and absorption corrections in determining absolute integrated intensities. In particular, absorption correction is difficult with an irregular shaped sample as shown in inset to the Fig. 1 .To circumvent these problem, we have refined the magnetic structure using the ratios of intensities between 2 and 25 K, *i.e* using $R = I(2\text{ K})/I(25\text{ K}) = 1 + I_M/I_N$, assuming the nuclear intensity, I_N, does not vary between 2 and 25 K. By using the ratios of intensities, one can exclude the artifacts due to the resolution effects in a triple axis spectrometers as well as absorption corrections. The intensity ratios measured for equivalent reflections and for repeated measurements of the same reflection were averaged together to give a mean value of the ratio and is shown in Fig. 7 together with the calculated ratios. The procedure for calculating intensity ratios is outlined below and has been implemented using MATHEMATICA [35].

The cross-section for the magnetic neutron scattering can be written as [36]:

$$\left(\frac{d\sigma}{d\Omega}\right)_{el}^{M} = (\gamma r_0)^2 N_M \frac{(2\pi)^3}{v_{0m}} \sum_{\vec{\tau}_m} |F_m(\vec{\tau}_m)|^2 \times \{1 - (\vec{\tau}_m \cdot \hat{\eta})^2_{av}\} \delta(\vec{k} - \vec{\tau}_m) \quad (1)$$

where

$$F_m(\vec{\tau}_m) = \frac{1}{2} g \left\langle \vec{S}^{\eta} \right\rangle f(\vec{\tau}_m) \sum_d \sigma_d \exp(i\vec{\tau}_m \cdot \vec{d}) \exp(-w_d)$$

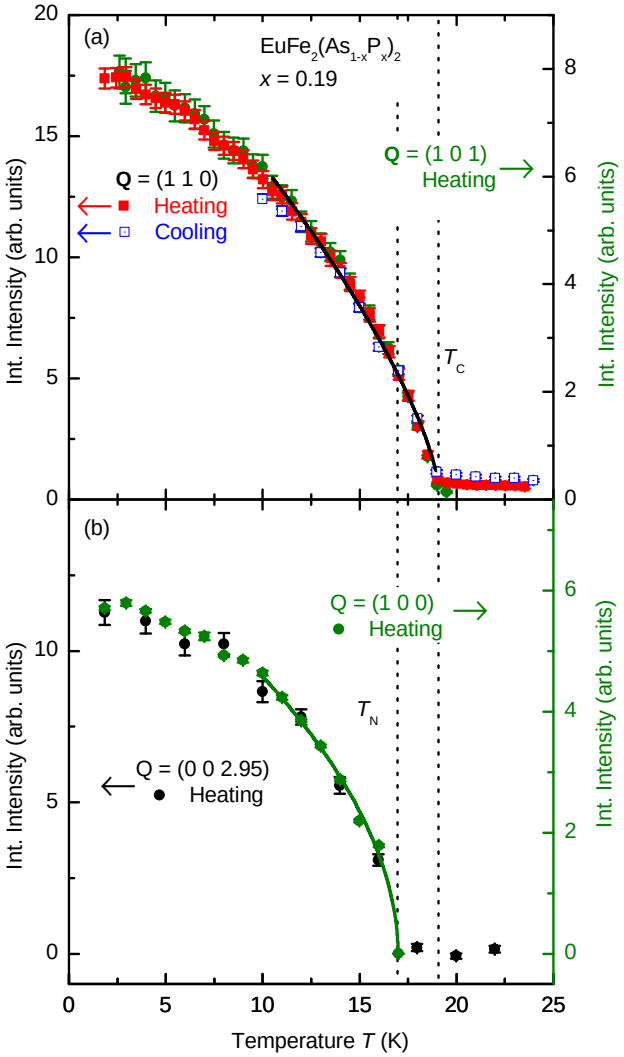

Figure 6: Temperature dependence of the integrated intensity for the (1 1 0) reflection measured during heating and cooling and for the (1 0 1) reflection measured during heating. (b) For comparison, we also show the temperature dependencies of the (0 0 2.95) and (1 0 0) reflections corresponding to the minor phase. The solid lines are fit to the data as described in the text.

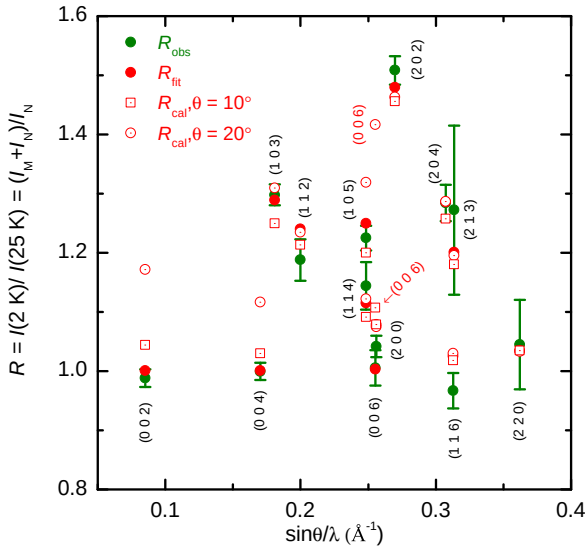

Figure 7: Comparison between the observed ratio (R_{obs}), fitted ratio (R_{fit}), and calculated ratio (R_{cal}) for the measured reflections. Details have been outlined in the text.

Table I: Parameters used for least square refinements of the ratios [13, 29]. Occupancies corresponding to the As and P sites were fixed according to the chemical composition.

Atom	Position in *I*4/*mmm*				B(Å^2)	*n*
	site	*x*	*y*	*z*		
Eu	2*a*	0	0	0	0.8	1.00
Fe	4*d*	$\frac{1}{2}$	0	$\frac{1}{4}$	0.3	1.00
As	4*e*	0	0	0.3615	0.3	0.81
P	4*e*	0	0	0.3615	0.3	0.19
	a = 3.91 (2) Å, *c* = 11.77(4) Å					

Here, $\gamma r_0 = 5.36 \times 10^{-15}$ m, N_M = Number of magnetic unit cell in the crystal, v_{0m} is the volume of the magnetic unit cell, $\vec{\tau}_m$ is the vector in magnetic reciprocal lattice, w_d is the Debye-Waller Factor (DWF). $\hat{\eta}$ is the direction of spin $\vec{S}$ where *"av"* means average over domains [37]. g is the Landé g-factor and $f(\vec{\tau}_m)$ is the magnetic form factor at the scattering vector $\vec{\tau}_m$. σ_d = 1 in this case and d denotes magnetic atoms in the magnetic unit cell.

Similarly, the coherent elastic nuclear scattering cross-section can be written as:

$$(\frac{d\sigma}{d\Omega})^N_{elastic} = N_N \frac{(2\pi)^3}{v_0} \sum_{\vec{\tau}_m} \left|F_N(\vec{k})\right|^2 \delta(\vec{k} - \vec{\tau}) \quad (2)$$

$$F_N(\vec{k}) = \sum_d \bar{b}_d \exp(i\vec{k} \cdot \vec{d}) \exp(-w_d)$$

where symbols have usual meaning similar to magnetic scattering and $\bar{b}_d$ is the nuclear scattering length for the d^{th} ion. The integrated intensity of a reflection at a scattering angle 2θ can be written as:

$$I = \frac{V}{v_0^2} \phi \lambda^3 \times A(\theta) \times B(\mu) \times y_s \times \frac{d\sigma}{d\Omega} \quad (3)$$

where V is the volume of the crystal, ϕ is the incident neutron flux, $A(\theta)$ contains angular dependent factors such as

Table II: The observed, fitted and calculated ratios for the reflections with magnetic contribution of $EuFe_2(As_{0.81}P_{0.19})_2$. Various cases have been considered as described in the footnote and in the main text.

h	k	l	$\sin\theta/\lambda$ Å^{-1}	R_{obs} $\times10^2$	${R_{fit}}^a$ $\times10^2$	${R_{fit}}^b$ $\times10^2$	${R_{fit}}^c$ $\times10^2$	${R_{fit}}^d$ $\times10^2$	${R_{cal}}^e$ $\times10^2$	${R_{cal}}^f$ $\times10^2$
0	0	2	0.0851	98.8± 1.4	100.1	100.0	104.2	111.7	104.4	117.1
0	0	4	0.1702	99.9±1.4	100.1	100.0	102.9	107.9	103.0	111.7
0	0	6	0.2553	100.6± 2.4	100.3	100.0	110.2	128.5	110.7	141.7
1	1	2	0.2000	118.8± 3.5	124.0	124.0	122.9	116.0	124.1	123.5
1	1	4	0.2485	114.4± 4.4	111.5	111.5	111.2	108.3	111.7	112.2
1	1	6	0.3129	96.7± 3.0	102.5	102.5	102.5	102.0	102.6	102.9
2	1	3	0.3134	127.2± 14.0	120.1	120.0	119.1	113.3	120.1	119.6
2	2	0	0.3620	104.5± 7.6	103.4	103.4	103.2	102.2	103.4	103.3
1	0	3	0.1808	129.8± 1.8	128.9	128.9	128.3	121.1	129.7	130.9
1	0	5	0.2483	122.5± 2.0	124.9	124.9	125.7	121.8	126.9	131.9
2	0	0	0.2559	104.2± 1.8	107.8	107.8	107.4	105.1	107.8	107.5
2	0	2	0.2698	150.9± 2.4	147.9	148.0	145.6	131.6	147.9	146.3
2	0	4	0.3074	128.4± 3.0	128.5	128.5	127.4	119.6	128.8	128.7
			Parameters:		m_{Eu} = 6.6(2) μ_B $\theta = 2(6)^\circ$	m_{Eu} = 6.6(2) μ_B $\theta = 0^\circ$	m_{Eu} = 6.5(2) μ_B $\theta = 10^\circ$	m_{Eu} = 5.5(5) μ_B $\theta = 20^\circ$	m_{Eu} = 6.6 μ_B $\theta = 10^\circ$	m_{Eu} = 6.6 μ_B $\theta = 20^\circ$
			Quality factors:		R_{wp} = 3.3% χ^2_R = 1.34	R_{wp} = 3.2% χ^2_R = 1.22	R_{wp}= 6.7% χ^2_R = 3.8	R_{wp} = 15.8% χ^2_R = 25.0		

[a]Fitted with m_{Eu} and canting angle θ, [b, c, d] Fitted with m_{Eu} and canting angle was fixed to 0°, 10°, 20°, respectively.
[e]Calculated with m_{Eu} = 6.6 μ_B and θ = 10°, [f]Calculated with m_{Eu} = 6.6 μ_B and θ = 20°.

$R_{wp} = 100\frac{\sum_n w_n |I^2_{obs,n} - I^2_{calc,n}|}{\sum_n w_n I^2_{obs,n}}$. $w_n = 1/\sigma^2_n$, is the weight where σ^2_n is the variance of $I_{obs,n}$.
$\chi^2_R = \frac{1}{N-p}\sum_n w_n (I_{obs,n} - I_{calc,n})^2$. p is the number of parameters, N is the total number of observations.

Lorentz factor, resolution factor and $B(\mu)$ is the absorption correction factor. The secondary extinction correction factor, y_s, depends on the mosaic width, scattering angle and average scattering cross-section for a particular reflection. It can be seen from Eqns. (1-3) that in the calculated ratio all factors except, (i) absolute value of the moment, (ii) moment direction, (iii) DWF and, (iv) extinction correction cancels out. However, in conventional single crystal neutron diffraction experiment on similar compounds it was found that the extinction corrections are small and we will neglect them in the subsequent analysis. Fitting the nuclear intensities at T = 25 K with and without an extinction parameter (not shown) clearly demonstrates that the extinction can be neglected. In fact, adding an extinction parameter worsen the quality of fit. For the accurate determination of the DWF, a conventional neutron diffraction experiment up to high **Q** is needed. We have used the DWF's for the parent compound [13] and used same DWF for P as for As. Furthermore, we have compared our results without applying any DWF and the results are the same within errors. For the estimation of the nuclear intensity, the z position of As, z(As), is required. Since the z(As) varies from 0.363 for the parent compound to 0.360 for the end-member, we have used 0.3615 for the calculation of the nuclear intensity. All the structural parameters used in the refinement are listed in Table I. We have excluded in the refinement the very weak nuclear reflections with very strong magnetic contributions such as (1 1 0), (1 0 1) and (2 1 1) since the intensity of these reflections slowly decreases above T_C. The resulting fitted ratios are shown along with observed ratios in Fig. 7. We obtained magnetic moment size of Eu^{2+}, m_{Eu} = 6.6(2) μ_B with a possible canting angle θ = 2(6)° with the aid of MATHEMATICA [35]. The magnetic moment size is close to the theoretically predicted value of 7 μ_B for a $J = \frac{7}{2}$ Eu^{2+} ion.

Here we note that the canting angle of 2° from the fitting of the ratios is much smaller than the reported values of Ryan *et al.* [29] as well as Nowik *et al.* [25] of approximately 20°. Therefore, we have considered five different scenarios, namely, (b-d) fitted the ratios with canting angle fixed to 0, 10 and 20°, respectively and (e-f) simulated the ratios with moment size fixed to 6.6 μ_B and two different canting angles, 10 and 20°, respectively. The simulated results are shown in Fig. 7 and both the fitted and simulated results are summarized in Table II. It can be clearly seen that the (0 0 L) reflections deviate strongly from the observed ratio if any canting angle is added. The deviation is strongest for the (0 0 6) reflection. Therefore, measurement of accurate integrated intensities for weak reflections such as (0 0 6) using a triple axis spectrometer provide strongest constraint on the canting angle. Fitting with any canting angle is poor as can be seen from the obtained ratios as well as agreement factors in Table II. Fitting without any canting angle ($\theta = 0^\circ$) produces the best χ^2_R for the calculated ratios. Therefore, we conclude that the canting angle is zero in the present case, *i.e.* moments are aligned along the **c** direction.

IV. CONCLUSION

In conclusion, the magnetic structure of the Eu^{2+} moments in superconducting $EuFe_2(As_{1-x}P_x)_2$ sample with $x = 0.19$ has been determined using neutron scattering. We conclude that the Eu^{2+} moments order along the **c** direction below T_C = 19.0(1) K with an ordered magnetic moment of 6.6(2) μ_B in the superconducting state. An impurity phase similar to the underdoped phase exists within the bulk sample which orders antiferromagnetically below T_N = 17.0(2) K. Further measurements are necessary to elucidate the exact nature of the minor phase. We found no indication of iron magnetic order, nor an incommensurate magnetic order of the Eu moments associated with the major phase. The proposed canted antiferromagnetic order could not be detected in the superconducting sample. It will be interesting to investigate Eu magnetic order for higher doping level in $EuFe_2(As_{1-x}P_x)_2$ system using single crystal neutron diffraction.

S. N. likes to acknowledge S. Zapf and M. Dressel for fruitful discussion. Work at Göttingen was supported by the German Science Foundation through SPP 1458.

* Electronic address: s.nandi@fz-juelich.de

[1] D. C. Johnston, Adv. Phys. **59**, 803 (2010).

[2] Y. Kamihara, T. Watanabe, M. Hirano, and H. Hosono, J. Am. Chem. Soc. **130**, 3296 (2008).

[3] H. Takahashi, K. Igawa, K. Arii, Y. Kamihara, M. Hirano, and H. Hosono, Nature **453**, 376 (2008).

[4] X. H. Chen, T. Wu, G. Wu, R. H. Liu, H. Chen, and D. F. Fang, Nature **453**, 761 (2008).

[5] Z.-A. Ren, W. Lu, J. Yang, W. Yi, X.-L. Shen, Z.-C. Li, G.-C. Che, X.-L. Dong, L.-L. Sun, F. Zhou, et al., Chin. Phys. Lett. **25**, 2215 (2008).

[6] F.-C. Hsu, J.-Y. Luo, K.-W. Yeh, T.-K. Chen, T.-W. Huang, P. M. Wu, Y.-C. Lee, Y.-L. Huang, Y.-Y. Chu, D.-C. Yan, et al., Proc. Natl. Acad. Sci. **105**, 14262 (2008).

[7] J. Guo, S. Jin, G. Wang, S. Wang, K. Zhu, T. Zhou, M. He, and X. Chen, Phys. Rev. B **82**, 180520 (2010).

[8] M. Rotter, M. Tegel, and D. Johrendt, Phys. Rev. Lett. **101**, 107006 (2008).

[9] H. S. Jeevan, Z. Hossain, D. Kasinathan, H. Rosner, C. Geibel, and P. Gegenwart, Phys. Rev. B **78**, 092406 (2008).

[10] K. Sasmal, B. Lv, B. Lorenz, A. M. Guloy, F. Chen, Y.-Y. Xue, and C.-W. Chu, Phys. Rev. Lett. **101**, 107007 (2008).

[11] R. Marchand and W. Jeitschko, J. Solid State Chem. **24**, 351 (1978).

[12] J. Herrero-Martín, V. Scagnoli, C. Mazzoli, Y. Su, R. Mittal, Y. Xiao, T. Brueckel, N. Kumar, S. K. Dhar, A. Thamizhavel, et al., Phys. Rev. B **80**, 134411 (2009).

[13] Y. Xiao, Y. Su, M. Meven, R. Mittal, C. M. N. Kumar, T. Chatterji, S. Price, J. Persson, N. Kumar, S. K. Dhar, et al., Phys. Rev. B **80**, 174424 (2009).

[14] Y. Xiao, Y. Su, W. Schmidt, K. Schmalzl, C. M. N. Kumar, S. Price, T. Chatterji, R. Mittal, L. J. Chang, S. Nandi, et al., Phys. Rev. B **81**, 220406 (2010).

[15] Y. Qi, Z. Gao, L. Wang, D. Wang, X. Zhang, and Y. Ma, New J. Phys. **10**, 123003 (2008).

[16] Z. Ren, Q. Tao, S. Jiang, C. Feng, C. Wang, J. Dai, G. Cao, and Z. Xu, Phys. Rev. Lett. **102**, 137002 (2009).

[17] C. F. Miclea, M. Nicklas, H. S. Jeevan, D. Kasinathan, Z. Hossain, H. Rosner, P. Gegenwart, C. Geibel, and F. Steglich, Phys. Rev. B **79**, 212509 (2009).

[18] T. Terashima, M. Kimata, H. Satsukawa, A. Harada, K. Hazama, S. Uji, H. S. Suzuki, T. Matsumoto, and K. Murata, J. Phys. Soc. Jpn. **78**, 083701 (2009).

[19] Y. Tokiwa, S.-H. Hübner, O. Beck, H. S. Jeevan, and P. Gegenwart, Phys. Rev. B **86**, 220505 (2012).

[20] H. S. Jeevan, D. Kasinathan, H. Rosner, and P. Gegenwart, Phys. Rev. B **83**, 054511 (2011).

[21] S. Nandi, M. G. Kim, A. Kreyssig, R. M. Fernandes, D. K. Pratt, A. Thaler, N. Ni, S. L. Bud'ko, P. C. Canfield, J. Schmalian, et al., Phys. Rev. Lett. **104**, 057006 (2010).

[22] S. Zapf, H. S. Jeevan, T. Ivek, F. Pfister, F. Klingert, S. Jiang, D. Wu, P. Gegenwart, R. K. Kremer, and M. Dressel, Phys. Rev. Lett. **110**, 237002 (2013).

[23] G. Cao, S. Xu, Z. Ren, S. Jiang, C. Feng, and Z. Xu, J. Phys.: Condens. Mat. **23**, 464204 (2011).

[24] A. Ahmed, M. Itou, S. Xu, Z. Xu, G. Cao, Y. Sakurai, J. Penner-Hahn, and A. Deb, Phys. Rev. Lett. **105**, 207003 (2010).

[25] I. Nowik, I. Felner, Z. Ren, G. H. Cao, and Z. A. Xu, J. Phys.: Condens. Mat. **23**, 065701 (2011).

[26] S. Zapf, D. Wu, L. Bogani, H. S. Jeevan, P. Gegenwart, and M. Dressel, Phys. Rev. B **84**, 140503 (2011).

[27] S. Nandi, W. T. Jin, Y. Xiao, Y. Su, S. Price, D. K. Shukla, J. Strempfer, H. S. Jeevan, P. Gegenwart, and T. Brückel, Phys. Rev. B **89**, 014512 (2014).

[28] W. T. Jin, S. Nandi, Y. Xiao, Y. Su, O. Zaharko, Z. Guguchia, Z. Bukowski, S. Price, W. H. Jiao, G. H. Cao, et al., Phys. Rev. B **88**, 214516 (2013).

[29] D. H. Ryan, J. M. Cadogan, S. Xu, Z. Xu, and G. Cao, Phys. Rev. B **83**, 132403 (2011).

[30] F. Kagawa, K. Miyagawa, and K. Kanoda, Nature **436**, 534 (2005).

[31] T. Brückel, D. Hupfeld, J. Strempfer, W. Caliebe, K. Mattenberger, A. Stunault, N. Bernhoeft, and G. McIntyre, Eur. Phys. J. B **19**, 475 (2001).

[32] S. Nandi, A. Kreyssig, Y. Lee, Y. Singh, J. W. Kim, D. C. Johnston, B. N. Harmon, and A. I. Goldman, Phys. Rev. B **79**, 100407 (2009).

[33] J. Rodríguez-Carvajal, Physica B **192**, 55 (1993).

[34] P. Coppens, L. Leiserowitz, and D. Rabinovich, Acta Crystallogr. **18**, 1035 (1965).

[35] Wolfram-Research-Inc., *Mathematica* (Wolfram Research, Inc., Champaign, Illinois, 2008), version 7.0 ed.

[36] G. L. Squires, *Introduction to the Theory of Thermal Neutron Scattering* (Cambridge University Press, 2012).

[37] In the calculation four possible orientational domains, (u v w), (-u v w), (u -v w) and (-u -v w), were considered,